JOURNAL OF SOLID STATE CHEMISTRY 37, 248–255 (1981)

Phenomenological and Structural Study of a Low-Temperature Phase Transition in the $PbZrO_3$–$PbTiO_3$ System

A. AMIN, R. E. NEWNHAM, AND L. E. CROSS

Materials Research Laboratory, The Pennsylvania State University, University Park, Pennsylvania 16802

AND D. E. COX

Physics Department, Brookhaven National Laboratory, Upton, New York 11973

Received January 14, 1980; in revised form October 2, 1980

The Landau–Ginsburg–Devonshire phenomenological theory has been applied to the $PbZrO_3$–$PbTiO_3$ crystalline solid solution system to explore the behavior of the rhombohedral–tetragonal morphotropic phase boundary in the region below room temperature. The theory suggests that morphotropy is preserved, i.e., that the phase boundary occurs at nearly the same composition right down to 0 K. The rhombohedral ($R3m$)–rhombohedral ($R3c$) phase transition was investigated for a composition $PbZr_{0.6}Ti_{0.4}O_3$ using neutron diffraction. Structures in both phases were refined by the Rietveld profile fitting technique. The transition behavior in this composition was indicative of a diffuse-type phase transition, with a transition temperature somewhere between 250 and 300 K. The diffuse nature of this transition is perhaps due to short-range ordering of Zr and Ti. However, powder neutron diffraction is not ideal for determining critical behavior; therefore, it is difficult to make a quantitative conclusion in this respect. Values of the spontaneous polarization were obtained from the (Zr/Ti) shifts, and compared to those deduced from phenomenological theory.

Introduction

The perovskite solid solution between antiferroelectric $PbZrO_3$ and ferroelectric $PbTiO_3$ (PZT) contains a number of extremely important compositions used in the electronics industry (*1*). Many piezoelectric devices are made from poled PZT ceramics with compositions near the morphotropic phase boundary (MPB), the rhombohedral–tetragonal phase transition boundary (Fig. 1), where electromechanical coupling coefficients are unusually high.

In this work we report the results of applying the Landau–Ginsburg–Devonshire theory to PZT compositions near the morphotropic phase boundary at 248, 98, and 8 K, and a neutron diffraction investigation of the structure of one such composition, $PbZR_{0.6}Ti_{0.4}O_3$ at 295 and 9 K.

From an X-ray and neutron diffraction study of $PbZr_{0.58}Ti_{0.42}O_3$ and $PbZr_{0.9}Ti_{0.1}O_3$ at room temperature, Michel *et al.* (*10*) concluded that the space groups were $R3m$ and $R3c$ respectively, the latter involving doubling of the unit cell edges. In a recent neutron diffraction investigation Glazer *et al.* (*11*) have confirmed the existence of a transition from $R3c$ to $R3m$ symmetry in $PbZr_{0.9}Ti_{0.1}O_3$ with increasing temperature

0022-4596/81/050248-08$02.00/0

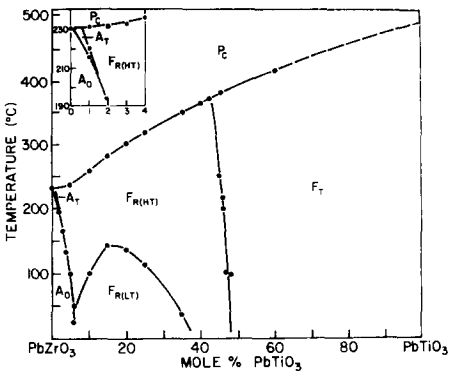

FIG. 1. $PbZrO_3$–$PbTiO_3$ phase diagram (after Jaffe *et al.* (*1*)).

between 60 and 100°C and have determined the cation displacements as a function of temperature between 25 and 250°C.

Based on the phase diagram in Fig. 1, there should be a rhombohedral–rhombohedral phase transition below room temperature near the morphotropic boundary. The low-temperature rhombohedral cell is twice the size of the high-temperature cell. Mechanical Q measurements by Kruger (*9*) seem to indicate such a transition. This is not, however, a reliable method of establishing phase boundaries.

To verify the existence of the transition we have done neutron diffraction experiments on $PbZr_{0.6}Ti_{0.4}O_3$ at two different temperatures (295 and 9 K). The structures were refined by the Rietveld method (*2*). Pyroelectric discharge experiments were carried out to explore the material response in the low-temperature region.

Landau–Ginsburg–Devonshire Phenomenology

For many ferroelectric crystals it has proved useful to correlate the dielectric, piezoelectric, elastic, and thermal properties of the paraelectric and ferroelectric phases by a thermodynamic free-energy theory. The Landau–Ginsburg–Devonshire (LGD) formalism gives an excellent description of these properties. A summary of past results can be found in the books on ferroelectricity by Jona and Shirane (*3*), Fatuzzo and Merz (*4*), and Lines and Glass (*5*).

Consider the free-energy function for a simple proper ferroelectric derived from a prototypic phase of symmetry $Pm3m$. For Brillouin zone center modes, the free energy may be written as a power series in dielectric polarization P (*6*, *7*) as follows:

$$\begin{aligned}\Delta G = {} & A(P_1^2 + P_2^2 + P_3^2) + B(P_1^4 + P_2^4 + P_3^4) + C(P_1^2P_2^2 + P_2^2P_3^2 + P_3^2P_1^2) \\ & + D(P_1^6 + P_2^6 + P_3^6) + E(P_1^4(P_2^2 + P_3^2) + P_2^4(P_1^2 + P_3^2) + P_3^4(P_1^2 + P_2^2)) \\ & + FP_1^2P_2^2P_3^2 - \tfrac{1}{2}S_{11}^P(X_1^2 + X_2^2 + X_3^2) - S_{12}^P(X_1X_2 + X_2X_3 + X_3X_1) \\ & - \tfrac{1}{2}S_{44}^P(X_4^2 + X_5^2 + X_6^2) - Q_{11}(X_1P_1^2 + X_2P_2^2 + X_3P_3^2) \\ & - Q_{12}(X_1(P_2^2 + P_3^2) + X_2(P_3^2 + P_1^2) + X_3(P_1^2 + P_2^2)) \\ & - Q_{44}(X_4P_2P_3 + X_5P_1P_3 + X_6P_1P_2), \end{aligned} \tag{1}$$

where A, B, C, D, E, and F are related to the dielectric stiffness and higher-order stiffness coefficients, S_{11}^P, S_{12}^P, and S_{44}^P are the elastic compliances measured at constant polarization, and Q_{11}, Q_{12}, Q_{44} are the cubic electrostriction constants in polarization notation. The expression is complete up to all six power terms in polarization, but contains only first-order terms in electrostrictive and elastic behavior.

Adjustable parameters in the free-energy function which fit the observed $PbZrO_3$–

$PbTiO_3$ phase diagram and the observed physical properties (dielectric, piezoelectric, and coupling coefficients) have been determined (*8*). Numerical values of ΔG for the tetragonal modification (*P4mm*) are plotted as a function of composition in Fig. 2 for three different temperatures (248, 98, and 8 K). The results are also given for the rhombohedral (*R3m*) and orthorhombic (*Bmm2*) cells. The rhombohedral–tetragonal degeneracy at the morphotropic phase boundary is temperature independent, as suggested by Fig. 1. The theory suggests that morphotropy is preserved; i.e., that the phase boundary between the tetragonal and rhombohedral phase fields occurs at nearly the same composition right down to 0 K.

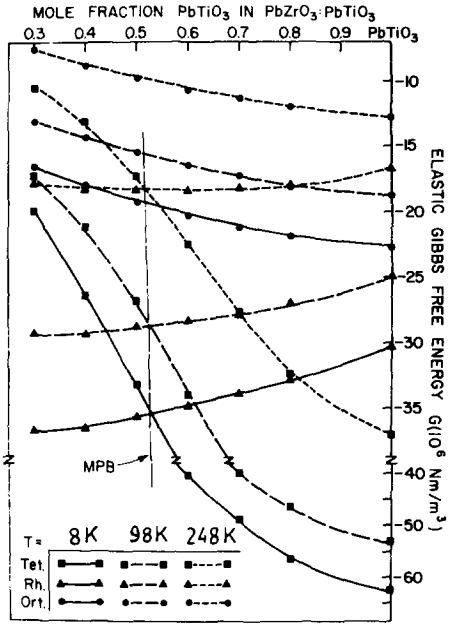

FIG. 2. Elastic Gibbs free energy as a function of composition across the single-cell region of the PZT phase diagram for three temperatures below room temperature.

Sample Preparation

The $PbZr_{0.6}Ti_{0.4}O_3$ sample used for the neutron diffraction powder pattern and the pyroelectric discharge experiments was prepared by a chemical coprecipitation method. The starting materials [spectroscopic-grade lead oxide, zirconium tetra-*n*-butoxide (ZBT) and titanium tetra-*n*-butoxide (TBT)] were weighed and blended with isopropyl alcohol in a mixer for 3 min while deionized water was slowly added. The white precipitated slurry was pan dried, then ball milled with ZrO_2 balls and distilled water for 8 hr. The product was again pan dried and calcined at 600°C for 6 hr, followed by regrinding and recalcination at 800°C for 3 hr. X-Ray powder patterns taken with Cu$K\alpha$ radiation showed sharp diffraction peaks up to high angles. There were no phases present other than rhombohedral (*R3m*) PZT.

Neutron Diffraction Studies

Data Collection

Neutron data from a $PbZr_{0.6}Ti_{0.4}O_3$ pellet were collected at the Brookhaven high-flux beam reactor at $T = 295$ and 9 K. Pyrolytic graphite in the (002) and (004) reflection positions were used as monochromator and analyzer, respectively. The neutron wavelength was 1.429 Å for the 9 K patterns and 1.650 Å for the 295 K pattern. Higher-order components were removed with a pyrolytic graphite filter. Data were collected at 0.05° intervals over each peak within a 2θ range 40–125° for the 295 and 9 K scans.

The 295 K data showed only reflections characteristics of the *R3m* symmetry ($a \sim 4$ Å), but at 9 K a number of extra reflections were observed. The extra reflections observed at 9 K could be identified as the $31\bar{1}$, $31\bar{3}$, $51\bar{1}$, 531, $53\bar{1}$, . . . , and others with h, k, and l all odd indexed on a doubled cell ($a \sim 8$ Å).

Structural Model and Data Reduction

Based on previous studies (*10, 11*), the

rhombohedral–rhombohedral transition was expected to stem from the tilt system $a^- a^- a^-$ [Glazer (*12*)] or $\phi\ \phi\ \phi$ [Aleksandrov (*13*)]. In the Glazer notation, the system of "rigid octahedra" tilts is represented by the symbol $a^i b^j c^k$ where a, b, and c represent rotations about the three pseudocubic axes. The superscripts i, j, and k denote the sense of rotations of adjacent corner-linked octahedra, such that + means the same sense, − means opposite sense, and 0 means no rotation. Therefore, the tilt system $a^- a^- a^-$ means three equal rotations of the Zr/TiO_6 octahedra about the pseudocubic axes ⟨100⟩, with neighboring octahedra rotating in opposite senses. The tilt system $a^- a^- a^-$ produces $R\bar{3}c$ (nonpolar) symmetry for the lower-temperature phase (9 K). However, since this transition is expected to be similar to those reported previously for other PZT compositions (*10, 11*), the structure was refined in space group ($R3c$). The polarity results from cation displacements along the rhombohedral [111] direction.

The $PbZr_{0.6}Ti_{0.4}O_3$ structures were refined by means of the profile-fitting technique (*2, 14*). The following scattering lengths were used: 0.94, 0.71, −0.34, and 0.58×10^{-12} cm for Pb, Zr, Ti, and O, respectively. The refined parameters included a scale factor, three half-width parameters defining the Gaussian line shapes, a counter-zero error, isotropic temperature factors, atomic coordinates, and unit cell parameters.

In the rhombohedral phases we chose to use the double pseudocubic cell ($a \sim 8$ Å). The fractional atomic coordinates of the $R3c$ phase are then given by (*21*).

	x	y	z
Pb	$\frac{1}{4} + s$	$\frac{1}{4} + s$	$\frac{1}{4} + s$
Zr/Ti	t	t	t
O	$-e + d$	$\frac{1}{4} - 2d$	$e + d$

s and t represent the fractional cation displacements along the three-fold axis, measured with respect to an origin lying midway between opposite faces of an oxygen octahedron. The parameter d is a measure of the octahedron distortion, which makes the upper and lower faces different. The e parameter indicates the rotation of an octahedron about the triad axis, with an angle of tilt ω, given by $\tan \omega = 4(3)^{1/2}e$.

In the $R3m$ phase there are no tilts, and e is equal to zero. The pseudocubic cell is not doubled in this phase, but to facilitate comparison of the two phases we also used a doubled cell to describe $R3m$. This was accomplished for $R3m$ by using the same symmetry operators used for $R3c$ and adding the constraint $x = y$ for the prototype oxygen atom, in addition to $x + y + z = \frac{1}{4}$.

Table I summarizes the refined parameters in each phase. The numbers between brackets represent the standard deviation in the least significant digit. Figure 3 shows calculated and observed intensity profiles for the two phases. The fit between observed and calculated profiles is quite good. The metal–oxygen bond lengths determined by neutron diffraction together with the sum of ionic radii "IR" of Shannon and Prewitt (*15*), are listed in Table II.

In addition, a limited amount of data was collected as a function of temperature with 2.46 Å neutrons. The evolution of the strongest superlattice reflection, pseudocubic (311), is illustrated in Fig. 4, and the integrated intensities normalized with respect to the fundamental (220) reflection are shown in Fig. 5. From this it can be inferred that the transition is unusually broad, and starts somewhat between 250 and 300 K. The analogous transformation in $PbZr_{0.9}Ti_{0.1}O_3$ is similarly rather poorly defined (*16, 17*).

Close inspection of the data taken at 295 K with 1.65 Å neutrons reveals a quite distinct modulation to the background scattering, as can be seen in Fig. 6 (lower

TABLE I

REFINED PARAMETER FOR $PbZr_{0.6}Ti_{0.4}O_3$

Temperature (K)	9	295
Shape parameters		
Phase	F_R (LT)	F_R (HT)
Space group	$R3c$ (C_{3v}^6)	$R3m$ (C_{3v}^5)
a_h (Å)	5.7597 (5)	5.7550 (4)
c_h (Å)	14.2510 (12)	14.2138 (11)
$2a$ (Å)	8.1730 (6)	8.1618 (4)
α (°)	89.614 (3)	89.676 (3)
Distortion parameters		
s	0.0343 (3)	0.0310 (4)
t	0.0114 (5)	0.0108 (7)
d	−0.0028 (1)	−0.0023 (1)
e	0.0105 (2)	—
ω (°)	4.2 (1)	—
Thermal parameters		
B (Pb)	0.57 (5)	1.9 (1)
B (Zr/Ti)	1.50 (2)	1.10 (17)
B(O)	1.24 (8)	1.57 (7)
Statistical parameters		
Number of parameters (P)	14	13
Number of observations (N)	802	934
Number of reflections	75	44
R_1 (%)[a]	1.68	4.85
R_2 (%)[b]	10.37	11.08
R_3 (%)[c]	11.70	14.28
R_{exp} (%)[d]	9.55	6.34

[a] $R_1 = 100\,\Sigma\,[I_{obs} - (1/c)I_{calc}]/\Sigma I_{obs}$.
[b] $R_2 = 100\,\Sigma\,[y_{obs} - (1/c)y_{calc}]/\Sigma y_{obs}$.
[c] $R_3 = 100\,\{\Sigma w[y_{obs} - (1/c)y_{calc}]^2\Sigma w[y_{obs}]^2\}^{1/2}$.
[d] R_{exp} (the expected R factor) $= 100\{(N - P + C)/\Sigma w[y_{obs}]^2\}^{1/2}$.

Note. I_{obs}, I_{calc} = observed and calculated integrated intensity of each reflection. y_{obs}, y_{calc} = observed and calculated profile data. w = weight allotted to each data point.

pattern). This type of modulation most likely arises from static displacements in preferred directions, since random displacements would simply lead to a monotonically increasing background, as is characteristic of thermal diffuse scattering. Calculations show that a simple model involving relaxation of about 0.1 Å of the six oxygen atoms in a TiO_6 octahedron towards

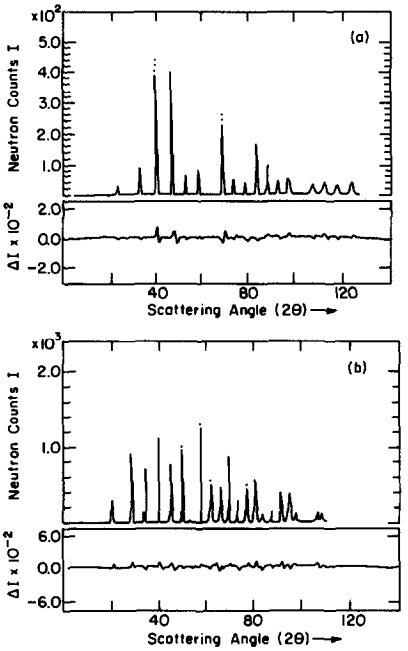

FIG. 3. Observed (dots) and calculated (full line) neutron intensity profile for the two phases of $PbZr_{0.6}Ti_{0.4}O_3$. The lower trace in each case is the difference between observed and calculated profiles. (a) F_R(HT) at 295 K; (b) F_R(LT) at 9 K.

the small Ti atom is qualitatively consistent with the general shape of the curve. However, the 221 K data from the temperature-dependence experiments which were obtained with much better counting statistics, show some structure in the Q range 0.9–0.3

TABLE II

METAL–OXYGEN BOND LENGTHS

Bond type[a]	Bond length (Å) T = 295 K	Bond length (Å) T = 9 K	Sum of "IR"
$Zr/Ti-O_1$	1.995	2.005	2.07
$Zr/Ti-O_2$	2.098	2.101	
$Pb-O_1$	2.912	3.041	2.89
$Pb-O_2$	2.515	2.481	

[a] O_1 and O_2 represent the oxygen atoms in the upper and lower faces respectively of an octahedron viewed along [111].

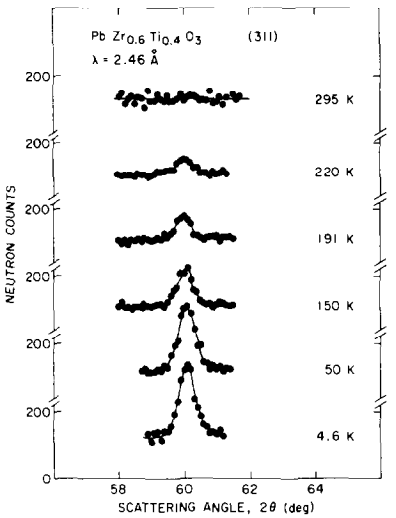

FIG. 4. Evolution of the pseudocubic (311) peak as a function of temperature. Data have been scaled for direct composition with the 4.6 K data, except for the 295 K results, which were obtained under slightly different conditions.

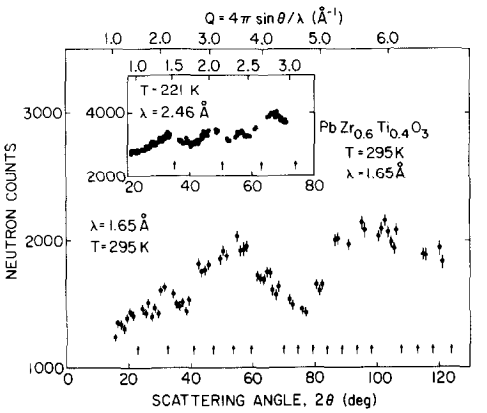

FIG. 6. Diffuse neutron scattering from $PbZr_{0.6}Ti_{0.4}O_3$. Lower diagram shows data taken at 295 K with 1.65 Å neutrons. Inset shows data taken with better counting statistics at 221 K with 2.46 Å neutrons. Gaps in data correspond to Bragg peaks. Arrows indicate peak positions derived from a primitive pseudocubic perovskite cell with a = 4.08 Å.

Å^{-1}, indicative of additional correlations (Fig. 6, inset). These may reflect short-range order which is a precursor of the tetragonal phase, or perhaps a tendency towards ordering of Zr and Ti.

Pyroelectric Discharge Experiment

The Chynoweth (*18*) technique used to explore the material pyroelectric response in the low-temperature region is shown in Fig. 7. The sample (a ceramic disk 2.8 mm

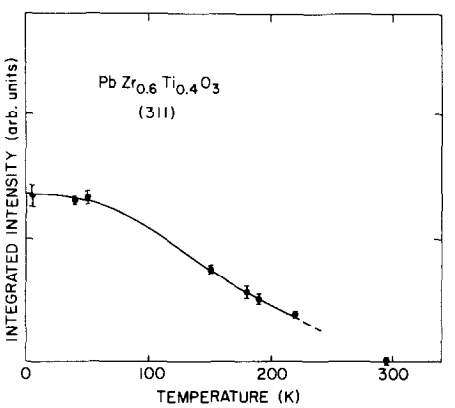

FIG. 5. Temperature dependence of the integrated intensity of the pseudocubic (311) reflection.

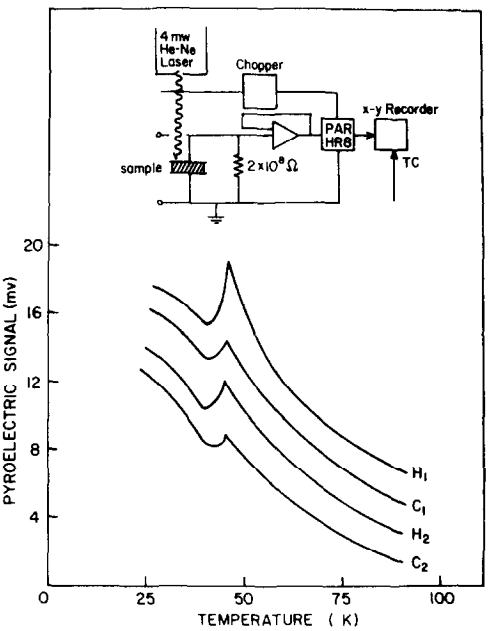

FIG. 7. Experimental arrangement and the pyroelectric signal as a function of temperature. The four curves represent successive heating and cooling cycles.

in diameter and 0.11 mm thick) was electroded with evaporated silver and mounted on a glass substrate. Using an electric field of 20 kV/cm, the ceramic was poled at room temperature. Carbon black was coated on the upper silver electrode to absorb light. The sample was then mounted in a recessed copper holder and cooled with liquid helium in an Air Products LT-3-110 cold finger. A buffer FET preamplifier positioned within the cold finger was used to minimize loading capacitance on the sample, thereby maintaining reasonable signal levels. The sample was irradiated by a chopped defocused 4-mW He–Ne laser and the pyroelectric signal detected with a lock-in amplifier (PAR-HR8). The level of pyroelectric signal (mV) as a function of temperature for two heating/cooling cycles (H_1, C_1) and (H_2, C_2) is shown in Fig. 7. The heating/cooling rates were about 4–5 K/min.

The observed peak in the pyroelectric signal around 50 K is not due to a ferroelectric–ferroelectric phase transition. It is probably due to (i) a relaxation effect in the sample as evidenced by the gradual decay of the 311 intensity in this temperature region; (ii) release of energy stored in a form of secondary cell activity involving oxygen vacancies which act as charge carriers and interact with the metal electrodes (*22, 23*). The laser beam chopper frequency is stable to ±0.1% in the frequency range 5–4000 Hz, therefore we exclude the nonuniform heating or cooling effect "false-pyroelectricity" (*24*) as a possible cause of the observed signal.

Correlation of the Spontaneous Polarization and Atomic Displacements

Based on a survey of 10 different ferroelectrics, Abrahams *et al.* (*19*) found that the spontaneous polarization P_s along the polar axis is linearly related to the homopolar atom shift δz (Å) by the relation

TABLE III

Zr/Ti Atom Shifts and Spontaneous Polarization

T (K)	Zr/Ti Shifts δz (Å)	P_s [111] from Eq. (2) (C/m_2-Å)	P_s [111] from (LGD) Eq. (1) (C/m_2-Å)
295	0.154 (9)	0.39 (3)	0.34
9	0.162 (7)	0.41 (2)	0.39[a]

[a] Taking into account the zone center mode only.

$$P_s = K\,\delta z, \qquad (2)$$

where $K = 2.58\ (9)\ c/m^2$-Å.

A slightly different value of $K = 2.51\ (7)$ was found to hold for the $PbZrO_3$–$PbTiO_3$ system (*20*). Table III shows a comparison between P_s [111] as calculated from Eq. (2) using the experimentally determined Zr/Ti shifts, and the P_s [111] values obtained from the (LGD) phenomenology. The agreement between the phenomenological P_s values and the values determined from Eq. (2) is quite good.

Summary and Conclusions

A rhombohedral ($R3m$)–rhombohedral ($R3c$) phase transition was found to occur in $PbZr_{0.6}Ti_{0.4}O_3$. The structures above and below the phase transition temperature were refined by the neutron profile fitting method (*2, 14*). The transition behavior in this composition shows more interesting features. It can be seen from Fig. 4 that the temperature dependence of the 311 intensity is rather unusual in that it does not approach the temperature axis very sharply to give a well-defined transition. The transition is unusually broad and starts between 250 and 300 K. The diffuse nature of this transition is perhaps due to short-range ordering of Zr and Ti. However, it is always difficult to separate Bragg- and diffuse-scattering components from powder data, therefore, it is premature to make any quantitative conclusions in this respect.

The Landau-Ginsburg-Devonshire (LGD) phenomenological results showed no anomalies of morphotropy compositions below room temperature. The spontaneous polarization values P_S as determined from the phenomenological theory are in surprisingly good agreement with the values calculated from the Zr/Ti shifts using Abrahams, Kurtz, and Jamieson's relation.

Acknowledgments

Ahmed Amin wishes to thank the Brookhaven National Laboratory for the kind hospitality during his stay there. This work was supported by the Office of Naval Research, Contract N00014-78-C-0291, and Division of Basic Energy Sciences, U.S. Department of Energy, under Contract EY-76-C-02-0016.

References

1. B. JAFFE, W. R. COOK, AND H. JAFFE, "Piezoelectric Ceramics," Academic Press, London/New York (1971).
2. H. M. RIETVELD, *J. Appl. Crystallogr.* **2,** 65 (1969).
3. F. JONA AND G. SHIRANE. "Ferroelectric Crystals," Pergamon, Oxford (1962).
4. E. FATUZZO AND W. J. MERZ, "Ferroelectricity," New York (1967).
5. E. M. LINES AND A. M. GLASS, "Principles and Applications of Ferroelectrics and Related Materials," Oxford Univ. Press (Clarendon), London/New York (1977).
6. A. F. DEVONSHIRE, *Philos. Mag.* **40,** 1040 (1949).
7. V. GINSBURG, *J. Exp. Theor. Phys. SSSR* **15,** 739 (1945).
8. A. AMIN, B. BADGER, JR., H. MCKINSTRY, AND L. E. CROSS, *J. Appl. Phys.*, in press.
9. H. A. KRUGER, "Final Technical Report," Clevite Corporation, Cleveland (1971).
10. C. MICHEL, J. M. MOREAU, G. D. ACHENBACH, R. GERSON, AND W. J. JAMES, *Solid State Commun.* **1,** 865 (1969).
11. A. M. GLAZER, S. A. MABUD, AND R. CLARKE, *Acta Crystallogr. Sect. B* **34,** 1060 (1978).
12. A. M. GLAZER, *Acta Crystallogr. Sect. B* **28,** 3384 (1972).
13. K. S. ALEKSANDROV, *Ferroelectrics* **14,** 801 (1976).
14. A. W. HEWAT, *J. Phys. C* **6,** 2559 (1973).
15. R. D. SHANNON AND C. T. PREWITT, *Acta Crystallogr. Sect. B* **25,** 925 (1969).
16. R. CLARKE AND A. M. GLAZER, *J. Phys. C* **7,** 2147 (1974).
17. D. BAÜRLE AND A. PINCUK, *Solid State Commun.* **19,** 1169 (1976).
18. A. G. CHYNOWETH, *J. Appl. Phys.* **27,** 78 (1956).
19. S. C. ABRAHAMS, S. K. KURTZ, AND P. B. JAMIESON, *Phys. Rev.* **172,** 551 (1968).
20. A. AMIN, R. E. NEWNHAM, AND L. E. CROSS, to be published.
21. H. D. MEGAW AND C. N. W. DARLINGTON, *Acta Crystallogr. Sect. A* **31,** 161 (1975).
22. J. D. HURD, A. W. SIMPSON, AND R. H. TREDGOLD, *Proc. Phys. Soc.* **73,** 448 (1959).
23. J. W. NORTHRIP, *Bull. Amer. Phys. Soc.* **4,** 424 (1959); *J. Appl. Phys.* **31,** 2293 (1960).
24. W. G. CADY, "Piezoelectricity," McGraw–Hill, New York (1946).